SUPERCRITICAL AIRFOIL SECTIONS WITH SLOTLESS FOWLER FLAPS FOR GLIDERS AND MOTORGLIDERS

by

Franz Georg Sator
Institut d'Aerodynamique
Ecole Polytechnique Federale de Lausanne

Presented at the XVIth OSTIV Congress
Chateauroux, France, 1978

INTRODUCTION

During the past few years, supercritical airfoil sections have become a subject of interest not only for designers of commercial aircraft, but for general aviation and motorglider designers also. In 1973, NASA started a new airfoil research program based on Whitcomb's 17% thick supercritical airfoil GA(w)-1[1]. The GA(w)-1 airfoil has already been used in several general aviation aircraft and motorgliders. In 1977, Dornier AG designed a 16% thick supercritical airfoil with a Fowler flap for use in a modified Skyservant[2]. In fact, the characteristics of thick supercritical airfoil sections indicate performance increases over conventional airfoil sections not only at transonic speeds, but also at low speeds.

The principal difference between conventional subsonic aerodynamic technology and supercritical technology lies in the cross-sectional profiles of lifting airfoils. At supercritical Mach numbers, a broad region of local supersonic flow extends vertically from both airfoils, as indicated by the pressure coefficients above the sonic value and by the shaded areas of the flow field shown in Fig. 1. This region of supersonic flow usually terminates in a shock wave, which causes an energy loss and therefore a drag increase. In addition, the shock wave produces a positive pressure gradient at the airfoil surface, which may cause separation of the boundary layer with an associated large increase in drag, severe airfoil buffeting, and stability and control problems. The much flatter shape of the upper surface of the supercritical airfoil reduces both the extent and strength of the shock wave, as well as the adverse pressure rise behind the shock wave, with the corresponding reductions in drag. To compensate for the reduced lift on the upper surface of the supercritical airfoil, resulting from the reduced curvature, the airfoil has increased camber near the trailing edge.

The characteristics of the supercritical airfoil suggest some potential benefits from applications to gliders and motorgliders. The supercritical airfoil may permit reducing structural weight by using thicker wing sections without penalizing aerodynamic performance. Another advantage of this airfoil appears at low speeds. Because of the much larger leading edge radius, it provides higher maximum lift than a conventional airfoil.

DESIGN CRITERIA

On the basis of performance calculations for gliders, the following design criteria for a basic airfoil of 17% have been fixed:

- minimum drag for lift coefficients in the range of $0.1 < c_\ell < 0.6$
- maximum lift of the basic airfoil (flaps in zero position): $1.6 < c_\ell < 1.7$
- maximum lift with flaps: $2.6 < c_{\ell max} < 2.7$
- pitching moment: $| c_{m_o} | < 0.1$

DESIGN PROCEDURE

Several theoretical methods and computer codes are in hand for analyzing the flow about a given airfoil, and for optimizing airfoils for a range of conditions. The theoretical analysis basically consists of calculating pressure distributions around arbitrary

airfoils, including viscous effects. The inverse problem is to calculate an airfoil from a desired pressure distribution, or other criteria. With today's computers, an experienced aerodynamicist can design a near optimum airfoil by an iterative approach which produces high performance over a broad range of operating conditions.

Our method is based on the small perturbation transonic potential equation in conservation law form

$$(K - (\gamma + 1) / 2 \cdot \phi_x^2)_x + \phi_{\tilde{y}\tilde{y}} = 0$$

$$\phi_{\tilde{y}x} - \phi_{x\tilde{y}} = 0$$

with the velocity components u and v in x- and y- direction

$$\phi_x = u \qquad \phi_{\tilde{y}} = v$$

and

$$K = \frac{1 - M_\infty^2}{M_\infty^{2\ 2/3}\ \sigma} \qquad \tilde{y} = (M_\infty^2 \sigma)^{1/3}\ y$$

The method involves iteration between the direct solution and the design solution. In the direct solution, the Neumann problem for the potential is solved. In the design step, the Neumann condition is replaced by a Dirichlet condition, that is: the pressure distribution is specified. Based on the irrotationality of the flow, the $\phi_{x\tilde{y}}$ in x-direction gives $\phi_{\tilde{y}}$, which is used in the same way as in the direct problem. After convergence, an integral boundary layer calculation is used to determine the displacement thickness and to correct the profile coordinates and the drag coefficient.

More details of the calculation procedure are given in Ref. 3.

Optimal wave drag in the transonic speed range has been used as design criteria for the basic airfoil. Only a few modifications have been made to adapt the airfoil shape to provide low speed, high lift characteristics.

OFF DESIGN CALCULATION

To calculate the complete polar of our designed airfoil, we need an analysis program capable of giving very accurate results not only for small angles of attack, but over the whole range in which the airfoil may be used. Observing that our small perturbation method fails for large angles of attack, we have used Garabedian's method[5]. This method is based on the full potential equation and involves the rapidly convergent finite difference scheme of E.M. Murman in a coordinate system tried out successfully by C.C.L. Sells. This involves mapping the exterior of the airfoil conformally onto the interior of a unit circle.

The analytic function which maps the interior of the unit circle $r < 1$ conformally onto the exterior of an airfoil in the (x,y) - plane, so that the origin corresponds to infinity, has the form

$$x + iy = F(r e^{it}) = \sum_{n=-1}^{\infty} a_n r^n e^{int}$$

The point $r = 1$, $t = 0$ corresponds to the cusp at the tail.

To remove the singularity in the potential at $r = 0$, we make the substitution

$$\phi = \frac{\cos(t + \alpha)}{r} + \phi$$

where α is the angle of attack. In terms of Sells coordinates t and r, the second order partial differential equation for the velocity potential becomes

$$(c^2 - \tilde{u}^2)\,\phi_{tt} - 2\,r\,\tilde{u}\,\tilde{v}\,\phi_{tr} + r^2(c^2 - \tilde{v}^2)\,\phi_{rr}$$

$$- 2\,\tilde{u}\,\tilde{v}\,\phi_t + r\,(c^2 + \tilde{u}^2 - 2\,\tilde{v}^2)\,\phi_r$$

$$+ r^{-1}\,(\tilde{u}^2 + \tilde{v}^2)\,(\tilde{u}\,\omega_t + r\,\tilde{v}\,\omega_r) = 0$$

where

$$\tilde{u} = \omega^{-1}\left[r\,\phi_t - \sin(t + \alpha)\right]$$

$$\tilde{v} = \omega^{-1}\left[r^2\,\phi_r - \cos(t + \alpha)\right]$$

$$\omega = r^2 \left| F' (r e^{it}) \right|$$

At $r = 0$ the velocity potential satisfies the boundary condition

$$\Phi = \frac{\Gamma}{2\pi} \tan^{-1} \left[\sqrt{1 - M_\infty^2} \tan (t + \alpha) \right]$$

involving the circulation Γ, and at $r = 1$ the Neuman boundary condition is fulfilled

$$\Phi_r = \cos (t + \alpha)$$

The circulation, which is a period of Φ, will be determined iteratively so that the Kutta-Joukowsky condition is satisfied at $t = 0$, $r = 1$

$$\Phi_t = \sin \alpha$$

For more details consult Ref. 5.

BOUNDARY LAYER CORRECTION

In order to use inviscid flow theory successfully in the design of airfoils, it is imperative that no significant boundary layer separation exists. If the boundary layer separates, it introduces a perturbation in shape caused by the wake. It is therefore necessary to calculate a boundary layer correction that will predict separation and indicate where the airfoil must be streamlined so as to moderate the adverse pressure gradient and bring the point of separation back to the last two or three percent of chord. Moreover, for lifting airfoils, even the very thin unseparated boundary layer diminishes the effect of the angle of attack and causes a smaller circulation because it is thicker on the upper surface than on the lower. Without a boundary layer correction, the only way to recover this loss is to increase the angle of attack and the free-stream velocity slightly. But the effects of such corrections are never certain.

To overcome these difficulties, our design program includes a laminar/turbulent boundary layer correction. The potential flow we compute is supposed to be the inviscid flow outside the boundary layer of an actual airfoil. To find the true airfoil generating our inviscid flow, it is necessary to subtract from the calculated streamline $\psi = 0$ a displacement thickness obtained from an appropriate boundary layer correction. For this purpose we use the integral method of A. Walz[6]/

This method is based on the differential equations of momentum thickness δ_2

$$\frac{d\delta_2}{dx} + \delta_2 \frac{du_\delta / dx}{u_\delta} (2 + \frac{\delta_1}{\delta_2}) - M_\delta^2 - \frac{\tau_w}{\rho_\delta u_\delta^2} = 0$$

and on the energy thickness δ_2

$$\frac{d\delta_3}{dx} + \delta_3 \frac{du_\delta / dx}{u_\delta} (3 + 2 \frac{\delta_4}{\delta_3} - M_\delta^2) - \frac{2}{\rho_\delta u_\delta^3} \int_0^\delta \tau \, d u = 0$$

To facilitate the mathematical treatment δ_2 is replaced by

$$Z = \delta_2 \, Re_{\delta_2}^n$$

where $n = 0.268$ for a turbulent boundary layer and the Reynolds number is

$$Re = \frac{u_\delta \cdot \delta_2 \cdot \rho_\delta}{\mu_w}$$

Introducing this, the equation of momentum thickness becomes

$$Z' + Z \frac{u_\delta'}{u_\delta} F_1^* - F_2 = 0$$

with

$$F_1 = 2 + n + (1 + n) \delta_1 / \delta_2 - M_\delta^2$$

$$F_1^* = F + n \frac{\mu_w' / \mu_w}{u_\delta' / u_\delta}$$

$$F_2 = (1 + n)\ \alpha\ \delta_2/(\delta_2)_u$$

The universal functions F_1 and F_2 may be evaluated independently of the specific problem if the form of the basic velocity profile in the boundary layer is known.

The derivative $\mu_w' = d\mu_w/dx$ of the molecular viscosity, the potential velocity $u_\delta(x)$ and the local Mach number $M_\delta(x)$ at the outer bound of the boundary layer, are known from the potential flow calculations.

The molecular viscosity may be calculated with the well known Sutherland formula

$$\frac{\mu}{\mu_\infty} = \frac{\rho_\infty}{\rho} \left(\frac{T}{T_\infty}\right)^{3/2} \cdot \frac{T_\infty + S\ T_\infty}{T + S\ T_\infty}$$

where T is total temperature and S is a constant equal to 0.3424.

With the shape parameter

$$H^* = \frac{\delta_3}{\delta_2}$$

the equation of the energy thickness may be written in the form

$$H^{*'} + H^*\ u_\delta'\ /\ u_\delta\ F_3 + F_4/Z = 0$$

The universal functions F_3 and F_4 are defined as

$$F_3 = 1 - \delta_1/\ \delta_2 + 2\ \delta_4/\delta_3$$

$$F_4 = \frac{c_f}{2}\ Re_{\delta_2}^n\ \left(2\ \frac{c_d}{c_f} - H^*\right)$$

$$= \frac{\delta_2}{(\delta_2)_u}\ (2\ \beta\ Re_{\delta_2}^{n-N} - \alpha\ H^*)$$

The parameters α and β are determined with a one parameter theory for the velocity profile. $N = 1$ for turbulent boundary layers.

More computational details of this integral method are given in Ref. 6. The method is valid up to the separation point.

THE SLOTLESS FLOWLER FLAP

Fowler flaps have been used for some tiem as landing aids and are usually built as slotted flaps. Because of the increase of drag, however, they are not suitable for glider application. Fowler flaps for gliders must have, at all deflections, a smooth surface variation without slots and other irregular surface modifications. An airfoil fulfilling these requirements has been developed by F.X. Wortmann[4]. It is a 17% thick airfoil with maximum camber at 43% and a 36% chord Fowler flap to change camber.

To avoid construction difficulties, we propose a 30% Fowler flap, where the flap deflection angle may be changed in the completely extended position. 10% of the Fowler flap is always outside the basic airfoil contour so that it may be used as a conventional flap to change camber of the basic airfoil.

AIRFOILS WITH SLOTLESS FOWLER FLAPS

For general application, it is suitable to use a set of airfoils of different thickness for variation in the spanwise direction. Therefore, a group of airfoils has been calculated with thickness between 17 and 12%. Special care has been taken to produce equivalent polars for the airfoils with similar shapes. Thus, it is possible to interpolate airfoils with equivalent aerodynamic characteristics.

The aerodynamic coefficients have been computed for a 17, 15, 13, and 12% thick airfoil in its basic configuration (Fowler flaps in zero position) and with Fowler flaps in fully extended position. No attention has been given to the change of camber of the 10% chord flap at the end of the Fowler flap which could be used to diminish drag at low lift coefficients.

The coordinates of the profiles are given in Table 1 where the first two numbers give the design year and the last three the thickness of the basic airfoil. The Fowler flap is always 30% chord. The polars are given in Figs. 2 to 5 with the Fowler flap in zero position and in fully extended position with a deflection of 20 degrees. A higher deflection may cause boundary layer separation on the upper surface as indicated by the boundary layer calculations.

In Fig. 6 the pressure distribution of

the 17% thick airfoil is compared with those of the GA(w) - 1 airfoil at 4 degrees angle of attack. The pressure peak at the nose has been diminished and on the lower side the pressure distribution has been filled up, resulting in a lower moment coefficient.

In Fig. 7 the polar of the 17% thick airfoil is compared with the FX 67-VG-170 of F.X. Wortmann. The maximum lift coefficient is higher but so is the minimum drag. This behaviour is to be expected because of the high lift design criteria of our airfoil and the minimum drag criteria for the FX 67-VG-170.

CONCLUSION

In general, our supercritical airfoils show a more gradual increase in velocity on the suction side than conventional Fowler flap airfoils. The pressure does not peak at the leading edge, but rather is distributed over the entire airfoil. Thus, lift is distributed over much more of the wing chord.

Since the drag is proportional to the square of the velocity, by reducing the size of the pressure peak, the drag is reduced. And, since the pressure is distributed farther over the airfoil surface, lift is increased.

This combination of reduced drag and increased lift results in smaller wings with less drag and less weight, or higher payloads may be carried as it has been demonstrated in motorgliders and two-place gliders for training purposes. The feasibility of such airfoils for highly efficient sailplanes remains to be demonstrated.

REFERENCES

1. McGhee, R.J. and Beasley, W. D.

   Low Speed Aerodynamic Characteristics of a 17% Thick Airfoil Section Designed for General Aviation Applications.

   NASA - TN -D 7428, 1973

2. Neue Technik Fur Sport- und Reiseflugzeuge.

   Flugrevue + Flugwelt 1/78, pp. 59-60.

3. Sator, F.G.

   Inverse Computation of Profile Shapes for Given Transonic Flow Configurations with and Without Detached Bow Shocks in Two Dimensional Turbomachinery Cascades.

   ASME - Paper No. 77-GT-33, 1977.

4. Wortmann, F.X.

   Airfoils for the Variable Geometry Concept.

   OSTIV - Publication XI, 1970.

5. Garabedian, P.R.; Korn, D.G.

   Analysis of Transonic Airfoils.

   Comm. Pure Appl. Math., Vol. 24, pp. 841-851, 1971.

6. Walz, A.

   Boundary Layers of Flow and Temperature.

   MIT Press, Cambridge, 1968.

x/c	y_u/c	y_l/c	y_u/c	y_l/c	y_u/c	y_l/c	y_u/c	y_l/c
0.00000	0.00000	0.00000	0.00000	0.00000	0.00000	0.00000	0.00000	0.00000
.00200	-.21387	-.00961	.01155	-.00829	.01023	-.00697	.00957	-.00631
.00500	-.02016	-.01425	.01813	-.01222	.01611	-.01020	.01510	-.00919
.01250	-.03041	-.02024	.02743	-.01726	.02445	-.01428	.02296	-.01279
.02500	-.04127	-.02653	.03728	-.02254	.03329	-.01855	.03130	-.01656
.03750	-.04929	-.03146	.04454	-.02671	.03979	-.02196	.03741	-.01958
.05000	-.05549	-.03518	.05016	-.02985	.04483	-.02457	.04216	-.02185
.07500	-.06501	-.04149	.05875	-.03523	.05248	-.02896	.04935	-.02583
.10000	-.07243	-.04634	.06544	-.03935	.05845	-.03236	.05496	-.02887
.12500	-.07837	-.05015	.07081	-.04259	.06325	-.03503	.05947	-.03125
.15000	-.08337	-.05350	.07531	-.04544	.06726	-.03739	.06324	-.03337
.17500	-.08768	-.05620	.07921	-.04773	.07075	-.03927	.06652	-.03504
.20000	.09125	-.05842	.08245	-.04962	.07364	-.04081	.06924	-.03641
.25000	.09689	-.06176	.08756	-.05243	.07823	-.04310	.07356	-.03843
.30000	.10077	-.06356	.09111	-.05390	.08144	-.04423	.07661	-.03940
.35000	.10315	-.06423	.09331	-.05439	.08346	-.04454	.07854	-.03962
.40000	.10406	-.06389	.09418	-.05401	.08430	-.04413	.07936	-.03919
.45000	.10363	-.06251	.09386	-.05274	.08409	-.04297	.07920	-.03808
.50000	.10179	-.06001	.09227	-.05049	.08275	-.04097	.07799	-.03621
.55000	.09831	-.05597	.08923	-.04689	.08016	-.03782	.07562	-.03328
.57500	.09591	-.05313	.08714	-.04436	.07837	-.03559	.07399	-.03121
.60000	.09294	-.04981	.08454	-.04141	.07615	-.03302	.07195	-.02882
.62500	.08937	-.04602	.08141	-.03806	.07344	-.03009	.06946	-.02611
.65000	.08533	-.04194	.07784	-.03445	.07036	-.02697	.06661	-.02322
.67500	.08078	-.03764	.07381	-.03067	.06685	-.02371	.06336	-.02022
.70000	.07578	-.03322	.06937	-.02681	.06296	-.02040	.05975	-.01719
.72500	.07041	-.02875	.06457	-.02291	.05874	-.01708	.05582	-.01416
.75000	.06467	-.02411	.05945	-.01889	.05423	-.01367	.05162	-.01106
.77500	.05869	-.01986	.05407	-.01524	.04945	-.01062	.04714	-.00831
.80000	.05253	-.01549	.04853	-.01149	.04453	-.00749	.04253	-.00549
.82500	.04612	-.01159	.04272	-.00819	.03933	-.00480	.03763	-.00310
.85000	.03956	-.00825	.03675	-.00544	.03394	-.00263	.03253	-.00122
.87500	.03292	-.00544	.03066	-.00318	.02840	-.00092	.02728	.00020
.90000	.02622	-.00335	.02448	-.00161	.02274	.00013	.02187	.00100
.92500	.01953	-.00236	.01824	-.00107	.01695	.00022	.01631	.00086
.95000	.01278	-.00248	.01189	-.00159	.01099	-.00069	.01054	-.00024
.97500	.00598	-.00390	.00540	-.00332	.00482	-.00274	.00453	-.00245
1.00000	-.00078	-.00779	-.00119	-.00738	-.00160	-.00697	-.00181	-.00676
	S 78-F-170		S 78-F-150		S 78-F-130		S 78-F-120	

Table 1 Coordinates of supercritical airfoils with slotless Fowler flaps

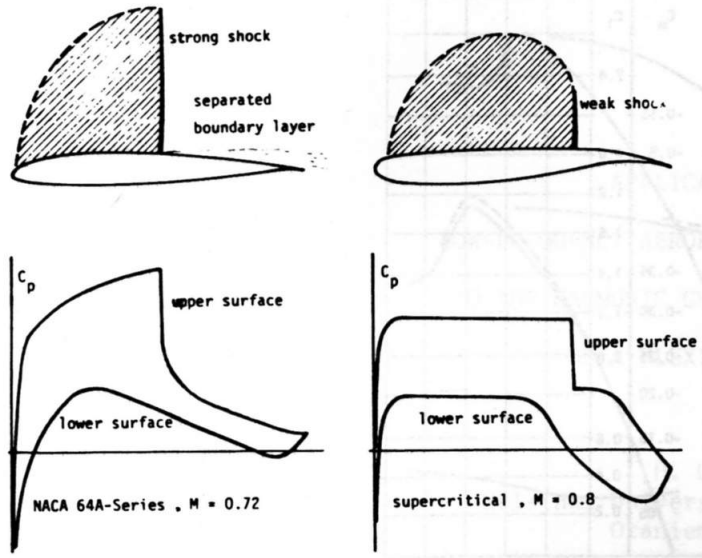

Fig. 1 Supercritical flow phenomena

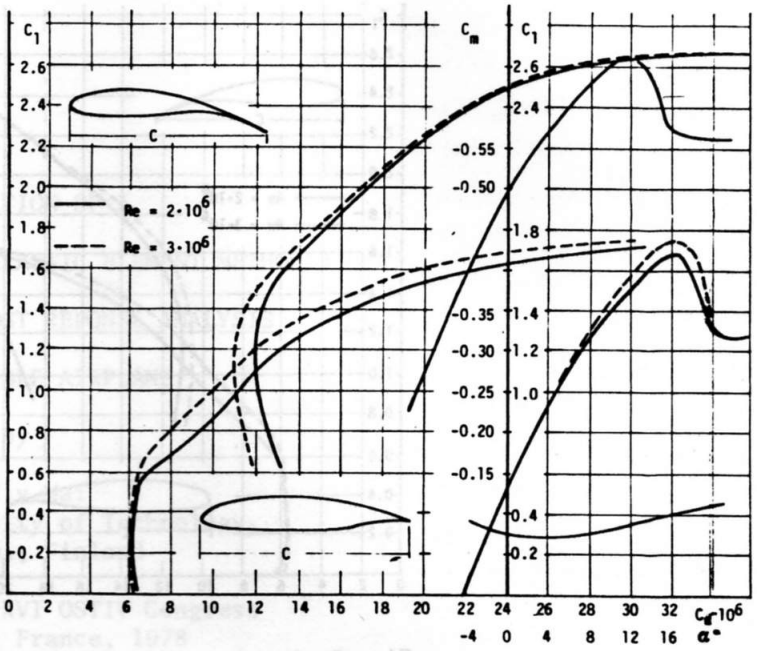

Fig. 2 Aerodynamic coefficients of S 78-F-170 airfoil

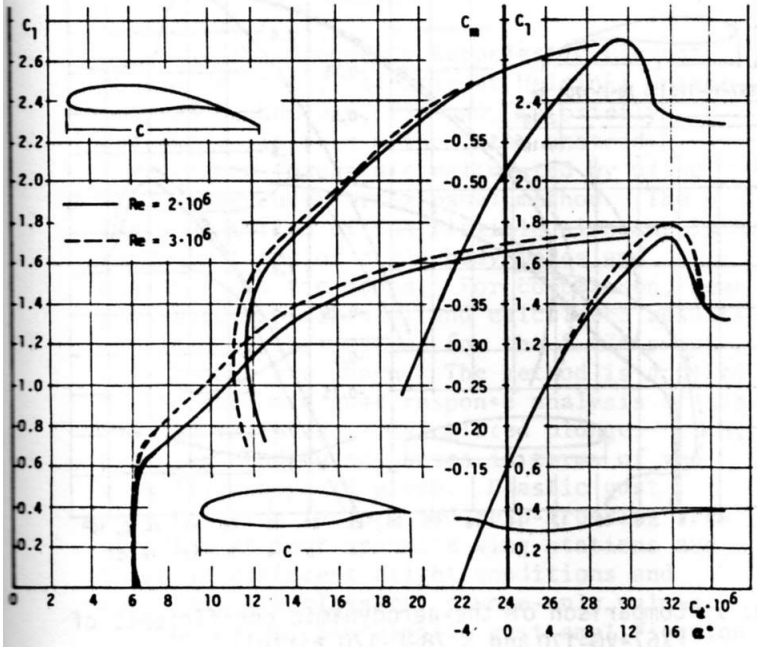

Fig. 3 Aerodynamic coefficients of S 78-F-150 airfoil

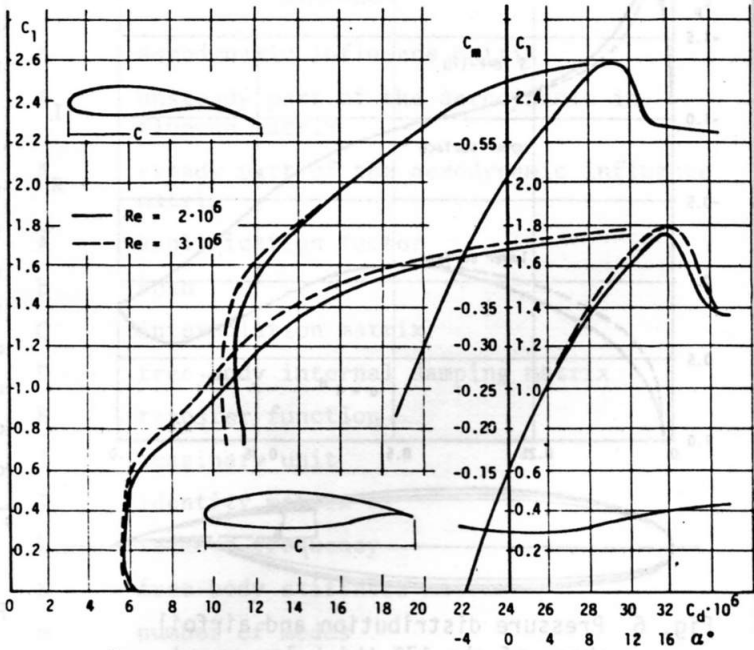

Fig. 4 Aerodynamic coefficients of S 78-F-130 airfoil

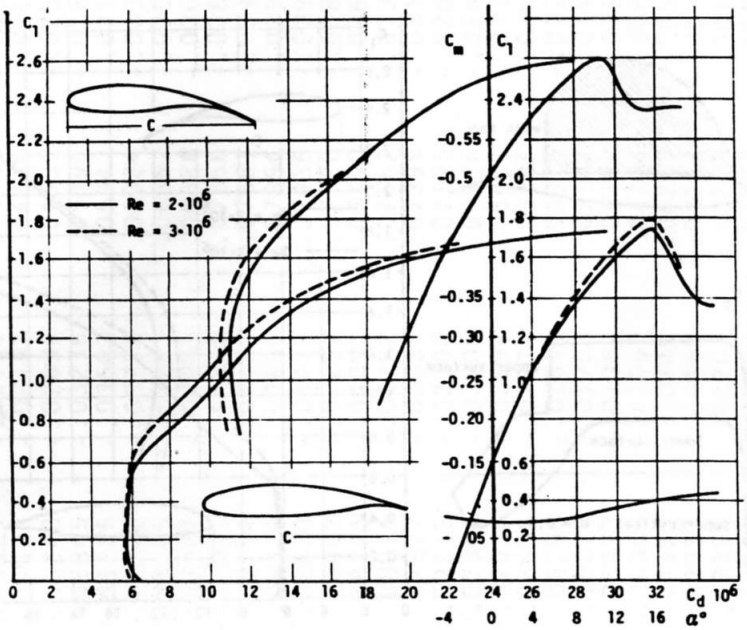

Fig. 5 Aerodynamic coefficients of S 78-F-120 airfoil

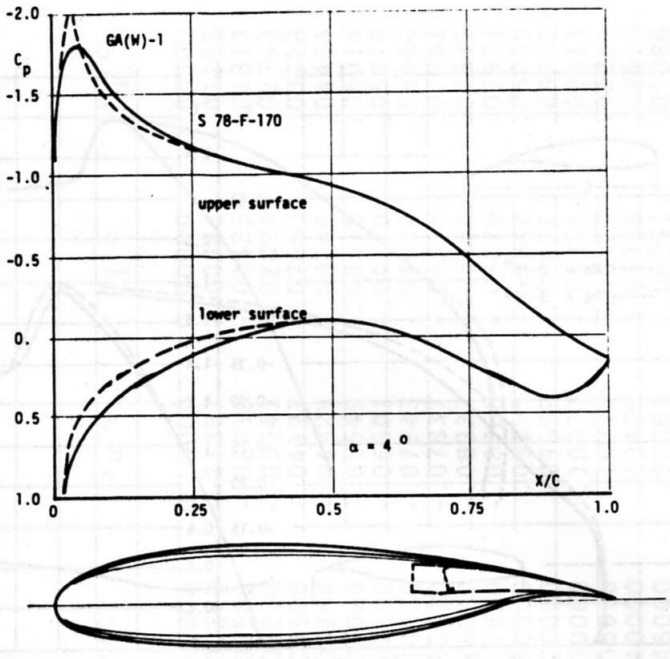

Fig. 6 Pressure distribution and airfoil shape of the 17% thick low speed supercritical airfoil (Fowler flap in zero position)

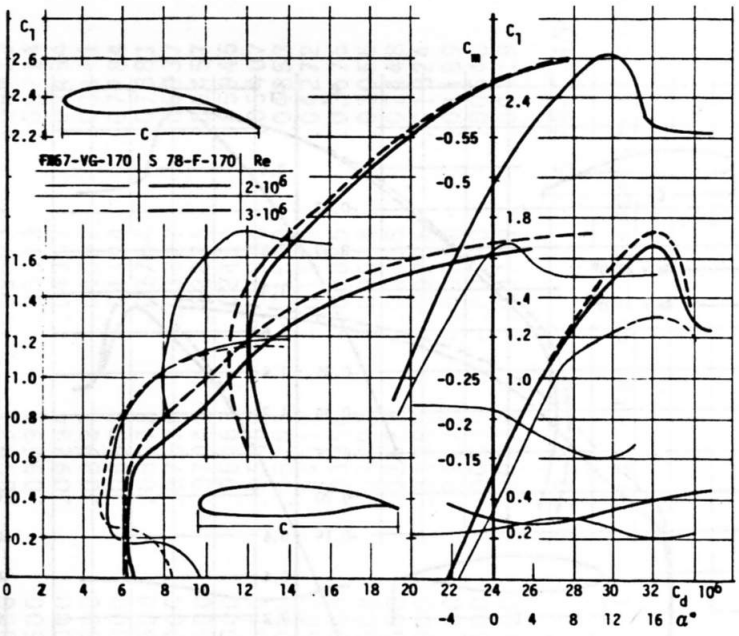

Fig. 7 Comparison of the aerodynamic coefficients of FX67-VG-170 and S 78-F-170 airfoil